HAL open science

Intrinsic properties controlling the sustainability of construction

Rachid Bennacer, Kamilia Abahri, Rafik Belarbi

To cite this version:

Rachid Bennacer, Kamilia Abahri, Rafik Belarbi. Intrinsic properties controlling the sustainability of construction. Elsevier. Sustainability of Construction Materials (second edition), 2016, 10.1016/B978-0-08-100370-1.00003-2 . hal-02465652

HAL Id: hal-02465652

https://hal.science/hal-02465652v1

Submitted on 4 Nov 2022

HAL is a multi-disciplinary open access archive for the deposit and dissemination of scientific research documents, whether they are published or not. The documents may come from teaching and research institutions in France or abroad, or from public or private research centers.

L'archive ouverte pluridisciplinaire **HAL**, est destinée au dépôt et à la diffusion de documents scientifiques de niveau recherche, publiés ou non, émanant des établissements d'enseignement et de recherche français ou étrangers, des laboratoires publics ou privés.

Distributed under a Creative Commons Attribution - NonCommercial 4.0 International License

Intrinsic properties controlling the sustainability of construction

R. Bennacer[*], *K. Abahri*[*], *R. Belarbi*[†]

[*]LMT-Cachan/ENS Cachan/CNRS/Université Paris Saclay, Cachan, France
[†]LaSIE, University of La Rochelle, La Rochelle, France

1 Introduction

Indoor air quality, healthy buildings, and material durability are important issues from both economic and social points of view. Construction materials, used externally or internally, can affect the health of building occupants as well as the energy consumption required while in service (eg, heating, hot water, air conditioning), thus its effect on the sustainability of the environment (International Energy Agency (IEA), 2007). Therefore, the preliminary selection of materials used for construction plays an important role in the success of the high environmental quality of building projects.

The normative rules (NF X 50-501, 1982) define durability as the ability of an entity to perform a function under given conditions of use and maintenance until the state limit is reached. More specifically, the durability of concrete is its ability to maintain its mechanical properties during its service life.

The durability is often concerned with the diffusion of harmful species into the building materials. For example, when talking about wood or reinforced concrete structures, the chloride penetration phenomena into concrete can't be ignored. Permeability is often associated with a material's durability as it relates to material diffusion. These two properties, diffusion and permeability, are interrelated; however, the question of their level of direct impact on material durability remains unclear.

In fact, very porous materials generally have pores at microscopic level, a complex and random pore structure where the role of heterogeneities becomes fundamental in the understanding of the physical phenomena involved and the prediction of behavior. Nevertheless, the heterogeneities related to the material morphology have not often been considered in the durability studies. In this context, the present chapter attempts to explore the link between the various physical properties of materials and their durability, while taking into consideration the material's morphological character, which is expressed in terms of porosity, as well as other phenomenon directly related to these properties.

2 Effect of physical properties on durability

A literature review on the different upscaling models (microscopic and macroscopic) of homogenization and the influence of materials and environmental parameters (temperature, relative humidity, pH, concentration, etc.) on durability are presented.

Porosity is an important factor that reflects the morphological property of each material that influences the material's durability and consequently its sustainability. Therefore, parameters affecting the porosity are highlighted in this section. The 2D (3D) porosity is defined as the ratio of area (volume) of pores divided by the total area (volume) of the material. Theoretically, two types of porosity can be observed:

- Total or absolute porosity that refers to the ideal porous medium where all the pores are interconnected because it considers all the pores including those that are not invaded by the fluid (ie, closed pores).
- The effective or accessible porosity, defined as the ratio of connected pores, through which the flow takes place in the total volume of the medium. This definition is used only if the structure of the porous medium is known.

Fig. 3.1 shows the various types of pores or voids in materials (see Ollivier and Torrenti, 2008, Benboudjema, 2012 for more details). It should be noticed that the connected open porosity (ie, open interconnected voids) has a major impact on the diffusivity value of the material. Descriptions of the various void/pores in the text is useful as indicated in Fig. 3.1.

The porosity in the heterogeneous material (cement paste in this case) is formed through non-connected air bubbles, the capillary porosity, and also the hydrates porosity. The cement paste has porosity at different scales of observation. Therefore, its experimental characterization requires the use of different investigative techniques to the desired level. Although these techniques often require a sample preparation prior to test (eg, predrying in the case of mercury-intrusion porosimeter testing), they provide an estimation of the size of the pores and their distribution. In fact, the coarseness of porosity is generally underestimated due to exaggeration from the so-called ink-bottle effect, in which pores are assimilated to cylinders and artifacts related to the preparation of the sample. This may cause alteration to the pore structure due to the drying technique, the very high mercury injection pressure, and also the hysteresis of the intrusion and the release of mercury. There are generally two types of pores:

- Capillary porosity vestige of the initial clinker porosity where the pore size ranges from 0.01 to 50 μm. It seems that the structural differences between the cement paste, of various water to cement ratios (W/C), is mainly derived from the differences in the capillary pores (Bouny, 2007).

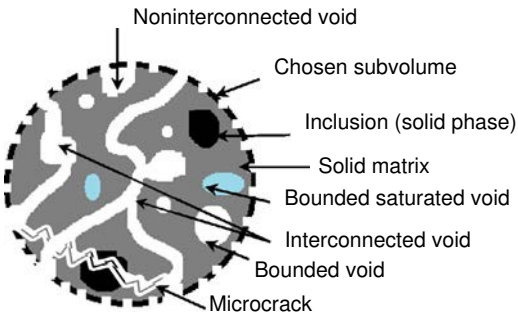

Fig. 3.1 Various porosities configurations.

- Gel C-S-H (calcium silicate hydrate) porosity which is the intrinsic porosity of hydrated products where the pores are small in size (ie, nanometer in size) where the dimensions range from a few angstroms to about 50–100 nm, which is much lower than that of the capillary porosity. These later can be further decomposed into interlamellar pores and intra-lamellaires cracks. This follows the C-S-H description adopted by various authors (Jennings, 2008; Nonat, 2004), but we can underline the limitation of continuous material approach on angstrom scale.

It is important to note that the C-S-H pores form a connected cluster, which is not generally the case for capillary pores, except for materials with very high W/C ratio. We have to underline that the mercury-porosimetry test shows tendency, but is unable to give quantifiable results at the necessary scale due to the high pressure used and the mechanical disorder that is caused.

The porosity of mortar and concrete is influenced by the evolution of microcracks during the early stages and the presence of aggregates. For compositions, W/C ratio of 0.4, containing silica fume and the mass ratio of the clinker by the silica fume is 10. The aggregates contact interface tends to increase the porosity to the surface of the grains through a destabilizing effect. On the other hand, portlandite appears preferentially in the vicinity of such an interface. This is obvious in Fig. 3.2A for materials without silica fume for different aggregate content (the W/C ratio is 0.4). For compositions containing silica fume (the weight clinker silica fume ratio is 10%) the coarse porosity (capillary) is higher when the aggregate content increases. This is less visible in the presence of silica fume (Garboczi and Bentz, 1992). The complex structure, time evolution, and the asymptotical porosity are related to the formulation and are predictable only for specific and chosen material.

3 Diffusion coefficient in cementitious materials

To ensure the sustainability of civil-engineering structures, knowledge of the properties related to diffusion is required. Diffusion refers to the transport process of a component in a given medium under the effect of its random agitation at the molecular level called Brownian motion (or vibrational on thermal aspect). If there are differences of concentration between two points in the medium, this phenomenon produces an overall transport component that is oriented from the most concentrated area to the least concentrated area. The diffusion process occurs even though the fluid (here water) doesn't move. Diffusion is a phenomenon that is irreversible in time. As it is difficult to follow the movement of each ion in a solution, the distribution is generally considered from a macroscopic point of view, that is to say that the overall particle motion is described by local concentration changes noted C. The ion will be described by its chemical potential ς by the relation:

$$\varsigma = \varsigma_0 + RT \ln C \tag{3.1}$$

where ς_0 is the chemical potential in a reference state, T is the absolute temperature, R is the gas constant and C is the concentration. The existence of a chemical potential

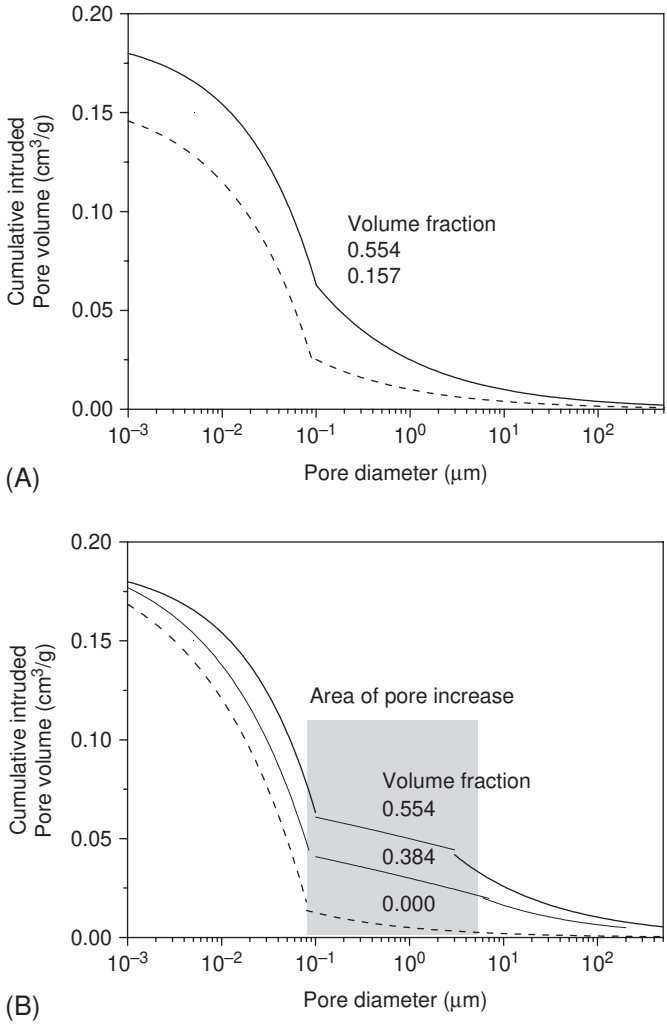

Fig. 3.2 Porosity distribution in pastes (A) and cement mortars (B) for different aggregate proportions.

gradient of a component i in a given medium causes a flow $\vec{J}$ of this component. The thermodynamics of this irreversible process postulates that there is a linear relationship between the flow and the chemical potential gradient acting as a thermodynamic force. Then we obtain the first Fick law, which gives the mass of solute per unit area and time[1]:

$$\vec{J} = -\rho D \vec{\nabla} C \tag{3.2}$$

[1] Could be written as $\vec{J} = -D\vec{\nabla}C$ where only the flux units change.

with D (m^2/s) being the diffusion coefficient of the species in the medium under consideration. The mass conservation in an infinitesimal volume element is expressed by the classical partial derivatives equation:

$$\frac{\partial C}{\partial t} = \mathrm{div}\left(D\overrightarrow{\mathrm{grad}}C\right) \tag{3.3}$$

In heterogeneous media, we can write $\boldsymbol{J}_{\mathrm{p}}$ ion flux passing through a defined unit area as follows:

$$\boldsymbol{J}_{\mathrm{p}} = -D_{\mathrm{e}} \cdot \vec{\nabla} C \tag{3.4}$$

where C is the average concentration on representative elementary volume (VER) and D_{e} is the effective diffusion coefficient (m^2/s). It is this factor that is accessed by the custom material without interaction between the diffusing species and the solid.

The ion flux through the material can be written by considering the material as a homogeneous medium or by considering the fact that the ions pass only through the porosity without integrating the complexity or tortuosity:

$$\boldsymbol{J}_{\mathrm{p}} = -D_{\mathrm{e}} \cdot \vec{\nabla} C = -D \cdot \phi \cdot \vec{\nabla} C \tag{3.5}$$

where

$$D_{\mathrm{e}} = \phi \cdot D \tag{3.6}$$

This shows that the effective diffusion coefficient D_{e} is lower than the clear fluid diffusivity (ie, diffusion coefficient D). So we keep in mind that in the case of pure fluid (at rest state), without electrostatic interaction between different ions, the diffusion through a liquid is related to the size of the spherical particles according to the Stokes–Einstein expression:

$$D = \frac{RT}{6\Pi N \mu a} \tag{3.7}$$

with μ being the water viscosity, a being the radius of the considered element and N being the Avogadro number. The principals' diffusivity values of different ions are given below (Table 3.1). As previously underlined and expected, the porosity has an important effect on the diffusivity value. Some authors (Benboudjema, 2012) collected

Table 3.1 Diffusion coefficient in pure water

Species	Diffusivity ($m^2 s^{-1}$)
HTO (tritium)	2.24×10^{-9}
Cl^-	2.03×10^{-9}
Ca^{2+}	1.56×10^{-9}

various results from the literature on effective diffusion-coefficient values (Fig. 3.3), whose principal product characteristics are given in Table 3.2.

Various changes in effective diffusivities as a function of porosity (accessible to water) on pastes and concrete based on cement and mineral additions are summarized in Fig. 3.3. It should be noted that the accessible porosity to water was

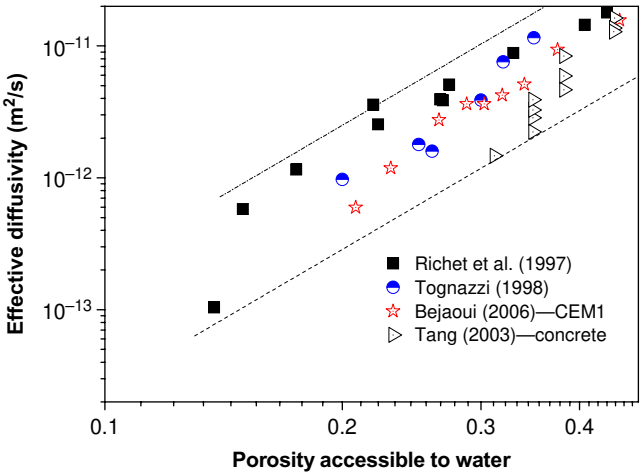

Fig. 3.3 Evolution of the effective diffusivity as a function of porosity for various cement pastes and concrete.
From Bogdan, M., 2015. Modélisation morphologique multi-échelles de matériaux cimentaires—application à la prédiction de propriétés effectives de diffusion (Thèse de doctorat de l'ENS de Cachan).

Table 3.2 Cement pastes and concrete diffusion coefficient

References	Cement type	Material type	Diffusing species
Richet et al. (1997)	CEM I	Cement paste	Tritiated water (T_2O)
Tits et al. (2003)	CEM I	Cement paste	
Bejaoui et al. (2006)	CEM I and V	Cement paste	
De Larrard (2010)	CEM I and fly ash (23% by mass)	Concrete	
Djerbia et al. (2008)	CEM I with silica fume (30% by mass)	Cement paste	Uranium
Tognazzi (1998)	CEM I	Cement paste	Leaching
Mejlhede Jensen et al. (1999)		Cement paste	Chlorides
Ngala et al. (1995)			
Tang (2003)		Concrete	
Carcassès et al. (2005)	CEM I, II, III, and IV		

From Bogdan, M., 2015. Modélisation morphologique multi-échelles de matériaux cimentaires—application à la prédiction de propriétés effectives de diffusion (Thèse de doctorat de l'ENS de Cachan).

calculated from the composition in the same case (Richet, 1992) tests and from the measurement of the mercury-porosimetry test. Under interactions between the chlorides and the cementitious matrix, the effective diffusion-coefficient evaluation was carried out using an isothermal interaction or by measuring the amount of flux through the sample.

Three mains findings can be extracted from Fig. 3.3:

- Except for chlorides, and therefore for tritiated water (T_2O) diffusivity, the use of mineral additives reduces the diffusivity dramatically by at least one order of magnitude.
- Generally, little difference exists between the cement paste and concrete, which may be due to the presence of the transition zone (aureole). Recent works minimize such assumptions (Bajja et al., 2015).
- In this case, the diffusion coefficient seems to be less dependent on the ions' nature.

Several results of the evolution of the effective chlorides diffusivity and various radionuclides of several results available from literature (the summary overview is described in Table 3.2) for different W/C ratio, different types of cement paste and concrete are grouped in Fig. 3.4. From these results the same conclusion obtained above can be confirmed, except that the effects of mineral admixtures seem even larger.

The effective diffusivity controls the diffusive process and the related material durability, but the weak level of diffusion amplifies the weight of transport phenomena induced by the flux over the material or flow over the porosity. The intensity of the flow and the ion diffusion amplification is related to the permeability.

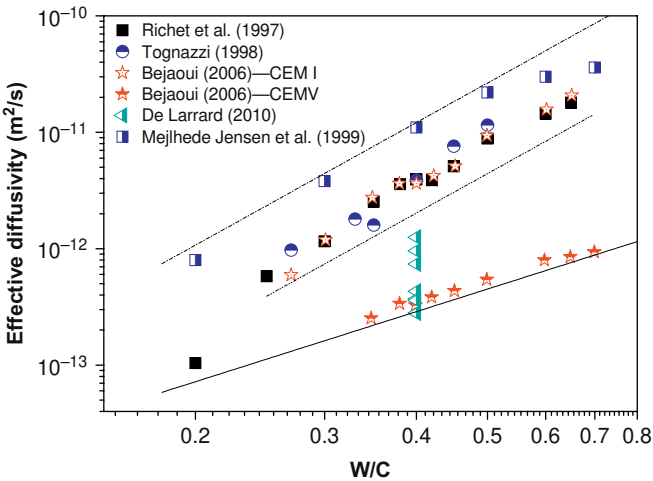

Fig. 3.4 Effective diffusivity evolution versus W/C ratio for different types of cement and concrete.

4 Correlation between porosity and permeability

A porous medium is primarily characterized by two interconnected macroscopic properties, which are porosity and permeability. Permeability is the fluid flow ability into a porous medium under the effect of a pressure gradient. The effective porosity gives an indication of the hydraulic permeability. However, the value of the permeability also depends on the pore structure, that is, interconnectivity and size distribution. The measured intrinsic permeability, in a given direction, is also relative to the open surface perpendicular to the fluid flow. Most porous materials have in fact a preferred orientation or an asymmetry of the porous phase in their structure, and the transmissibility of the saturated fluid does not happen in the same way in all directions. So as permeability or thermal conductivity change in direction, then the medium is anisotropic with respect to this property at the considered point.

A porous structure is considered heterogeneous if the property varies depending on the position of the point where it is located within the structure. Thus, in a porous material composed of several vertical isotropic porous layers, the properties such as permeability and thermal conductivity vary from one layer to the other, and constitute a generally heterogeneous porous medium. Furthermore, a porous medium is also heterogeneous because it is composed of a solid phase and a fluid phase (liquid/vapor/dry air). The porous medium is locally heterogeneous due to the large variation in characteristics that may exist within the solid matrix itself (eg, grains or fibers), as shown in Fig. 3.5. The homogenization technics allow for finding the condition to get globally homogeneous materials (on VER).

In addition to the high heterogeneity and anisotropy of most porous building materials, the latter contain localized cracks (Fig. 3.5B and C), which can influence the diffusion and especially the material permeability. Thus, there is a need to understand these phenomena by investigating the effective permeability, which is the principal parameter reflecting flow in porous media. Cracks represent preferential flow paths for the transport of fluid species and strongly contribute to the deterioration of structural

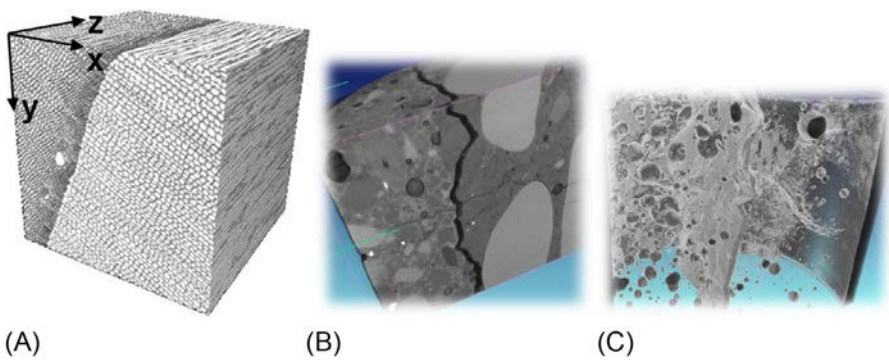

Fig. 3.5 Example of a locally heterogeneous and anisotropic porous media: (A) a 3D view of the spruce wood (B) and (C) cracked concrete with microbubbles.

performances by enhancing the apparent diffusive coefficient (eg, corrosion, carbonation, etc.) and safety (eg, radioactive fluid loss, radionuclide migration, etc.).

For example, in a recent study (Rastiello et al., 2015), investigation showed the effect of permeability on the fracture characteristic of porous materials where the mesoscale analyses of cracked porous volumes were performed. Mesostructures are defined according to the morphological framework proposed by Adler (2008), and recently developed by Roubinet et al. (2010). Several structures with different porosity are studied. They considered a cubical heterogeneous domain defined volumetrically by either a solid or fluid point defined as voxel information (Fig. 3.6). Each voxel represents an element of the solid matrix of the material and by consequence it represents the material morphology.

An explicit realization is given in Fig. 3.6 for different porosity from highly porous (0.7) to relative dense domain (0.05). This structure is obtained and characterized using three correlation lengths (6, 20, and 30) as shown from the granulometry illustrated in Fig. 3.7A (Bogdan, 2015).

The corresponding specific area (the interface between the solid structure and fluid subdomains) is shown in Fig. 3.7B where a maximum versus porosity is observed, which is due to percolation between dispersed solid grains and fluid channels. Such a specific-area is obtained through the analytical approach (Bogdan, 2015).

The porosity is also accessible analytically and checked numerically by integrating the solid and fluid phases associated with voxels information (see Fig 3.7B). Nevertheless in the statistical definition of the structure used it was found that the experimental values fit well with the porosity prediction. However, the computed minimum and maximum open sections (fluid plan in a given position) in comparison with the average section of the porosity domain (corresponding to global porosity) exhibit a constant difference for the different thresholds. Such deviation corresponds to the chosen variation and correlation length.

The relative variation of the porosity value increases as the threshold (or porosity) decreases (Fig. 3.7B). Based on known structure and geometrical information (eg, area, porosity, specific area), and by using the direct numerical simulation model, the equivalent thermal conductivity (or molecular diffusion) and permeability can be evaluated.

In this part, transport through macropores and cracks, as well as the diffusion in microporous solid inclusions, are taken into account. Uncracked porous volumes are considered first as a reference case. The pressure drop is normalized by the identified

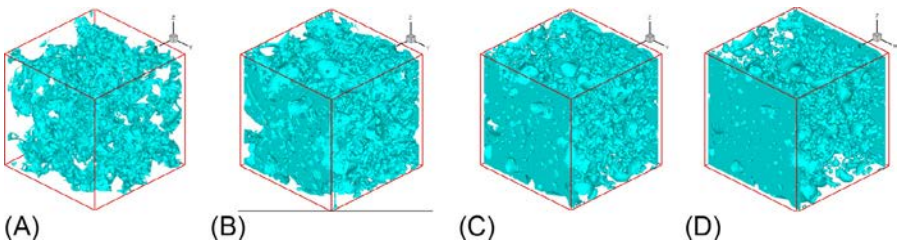

Fig. 3.6 3D field, from a strongly porous domain (A) reference case; to less porous: (B) 0.2; (C) 0.1; and (D) 0.05 (weak porosity).

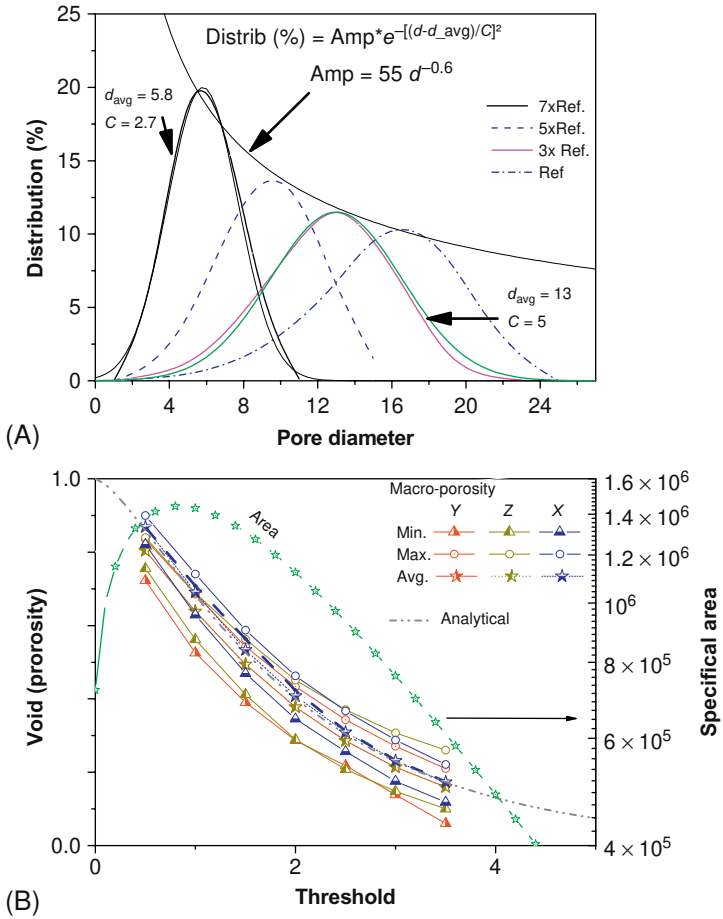

Fig. 3.7 Pore size distribution (A) and volumetric and surface porosity (B) versus the threshold level (complementary with Rastiello et al., 2015).

homogeneous permeability weighted by velocity term (V/Da), where Da is the Darcy number, a nondimensional parameter, representing the ratio of the permeability on the square passage section.

The cracks width effect on the average pressure gradient corresponding to two values of flow rates; 1 and 10 are illustrated in Fig. 3.8 for a porosity of 0.48. The pressure drop is normalized by the previously identified homogeneous permeability.

For microcracks the global flow doesn't change and remains horizontal and perpendicular to the section, and the pressure difference coincides with those obtained in the homogeneous case. For cracks with a width larger than 3% of the whole domain size (fluid and solid voxel ratio: 6/200), the apparent relative permeability changes. It can be observed that there is an excellent predictability of the pressure drop based on the previously identified permeability that is illustrated by the nonvisible effect of imposed flow rate (1 and 10). Such results can be expressed by an anisotropic tensor.

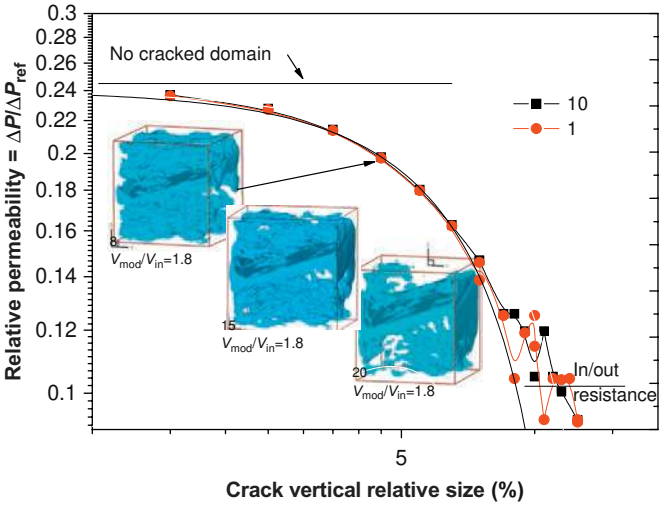

Fig. 3.8 Equivalent hydraulic permeability versus structure porosity (Rastiello et al., 2015).

When the crack width increases, the porous volume becomes more permeable as illustrated by the decrease in the pressure difference. For cracks having width larger than 15% of the global domain size, the pressure decrease exhibits asymptotical behavior resulting mainly from the entrance and exit of the fluid gaps and the crack channel. For such situations or intermediate crack widths a more complex phenomenon occurs with significant flow redistribution that affects the pressure-flow interlink. The flow change will induce a significant change in mass diffusion. In nonsaturated concrete, we face a more complex multiphase (liquid–gas) water distribution and time evolution. The complex phenomena evolve over time and are also interlinked with the temperature field.

5 Heat and mass interlinking

Heat transfer can also be appreciably affected by the morphology of the porous matrix and therefore its porosity, as mentioned above for fluid flow. Thermal conductivity is generally the most used parameter to describe heat transfer.

The models used to evaluate the effective thermal conductivity are very often based on the identification of the porous medium with a regular, simple geometric structure. Then, the conductivity is calculated by rigorous theoretical resolution, or by numerical calculation using simplifying assumptions. In the latter case, more formulations are obtained in explicit equivalent thermal conductivity (λ^*), which depends on the conductivity of the two solid–fluid phases and the porosity. The comparison of this training with experimental data is presented for fixed porosity in Fig. 3.9.

The existing expression remains inaccurate and unable to predict the equivalent thermal conductivity, the diffusivity, and the permeability. Several approaches

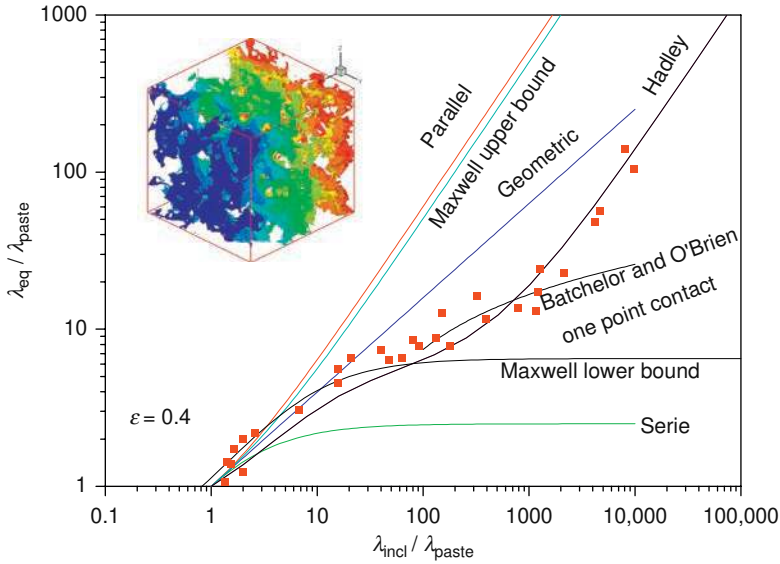

Fig. 3.9 Effective thermal conductivity for particle beds: theoretical prediction and experimental results (Kaviani, 1991).

including the porosity, tortuosity, or more complex structural parameters, allow some improvement with complex fitting. Based on the previously defined structure and known porosity, interface area (A_1), granulometry, and transverse surface, we will present a simplified scheme allowing for equivalence (for more detail see Rastiello et al., 2015).

The considered domain can be presented as three vertical multilayers where the central is a porous media of width $1/2e_0$ between two identical gaps of width e_0. The equivalent thermal scheme is series of three thermal resistances with the equivalent central as parallel thermal resistance composed by the fluid and solid phases. The geometrical ratio between the two parallel phases is given by the porosity ε. We insist on the interfacial fluid–solid area (A_1) controlling the coupling between the solid and fluid phase and the tortuosity. The equivalent, simplified resistance is given according to the following equation:

$$\frac{\lambda_f}{\lambda_{eq}} = 2e_0\left(1+\frac{\left(1/2e_0-1\right)}{\varepsilon+\left(1-\varepsilon\right)\lambda_r}\right) \tag{3.8}$$

with

$$\text{When } \lambda_r \to 0: \quad \frac{\lambda_f}{\lambda_{eq}} \to 2e_0\left(1+\frac{\left(1/2e_0-1\right)}{\varepsilon}\right) \tag{3.9}$$

and

$$\text{When } \lambda_r \to \infty: \quad \frac{\lambda_{eq}}{\lambda_f} \to \frac{1}{2e_0} \tag{3.10}$$

where $\lambda_r = \lambda_s / \lambda_f$. The analytical apparent conductivity is given by $\lambda_{eq}^{r} = \frac{\lambda_{eq}}{\lambda_f}$.

The obtained effective conductivity ratio for the different thresholds and solid–fluid conductivity ratio are shown in Fig. 3.10. The apparent conductivity increases with the increase in solid–fluid conductivity ratio. For high porosity ($\varepsilon = 0.7$, ie, threshold 3), the apparent thermal conductivity change with a ratio of two when the relative conductivity changes by the order magnitude of 10^2. For low porosity, the change is more pronounced. The obtained numerical results do not fit with the analytical part and do not tend to with the two-limit cases, represented on lower part of Fig. 3.10. This is illustrating the more complex phenomenon that is resumed by either the important part of the interfacial surface exchange (specific area) allowing the thermal coupling between the two considered phases in the intermediate transitional domain and the tortuosity of the solid or the fluid phases on the two asymptotical cases.

$$\lambda_r \to 0 \quad \frac{\lambda_f}{\lambda_{eq}} \to \underbrace{2e_0\left(1 + \frac{\left(1/2e_0 - 1\right)}{\varepsilon}\right)}_{\text{Corrected by tortuosity}} \tag{3.11}$$

$$\lambda_r \to \infty \quad \frac{\lambda_{eq}}{\lambda_f} \to \frac{1}{2e_0} \tag{3.12}$$

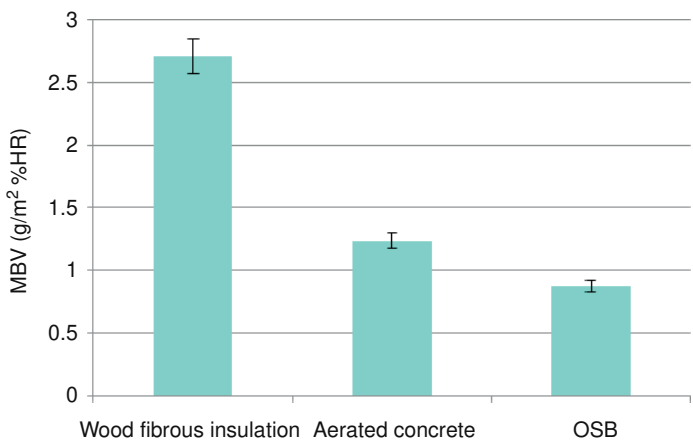

Fig. 3.10 Moisture buffer value of wood fiber insulation, cellular concrete, and OSB obtained after three cycles of wetting–drying.

Therefore, the ability to generate a controlled porous structure with known porosity and specific area is demonstrated. The porosity evolution modifies the apparent granulometry, the specific area, and the tortuosity. Moreover, in multiphase fluid (Bories et al. (2008)), the adsorption and capillary pressure modify local constraint and affect the previous underlined geometrical characteristic.

6 Vapor–liquid interaction

This section is concerned with the vapor–liquid interaction inside a material. Such interaction is related to the previous diffusion and permeability but could illustrate strong correlation with the physical and chemical adsorption phenomena. Physical adsorption involves the condensation of molecules on the surface of the solid material. Adsorbed molecules are weakly linked to the solid by intermolecular forces of attraction (mainly van der Waal's forces). The energy involved is <20 kJ/mol. There are no privileged sites and adsorption can be multimolecular, that is, that a second layer, then a third, can come to adsorb on the first. It is a reversible phenomenon since the adsorption is little influenced by the nature of the surface.

Chemical adsorption is due to ionic or covalent chemical bonds between gas and solid surface. This implies a change in its structure or reactivity. The energies involved are more important. They vary from 80 to 400 kJ/mol. Chemical adsorption can be monolayer. It is an irreversible phenomenon that is specific because it depends on the nature of the chemical bonds that the atoms in contact may contract.

Such adsorption and desorption processes could be seen as the effect of the environment on the materials, but due to the water contain reversibility, it could be analyzed as a material contribution in regulating the ambient building vicinity.

The material contribution in regulating the ambiance vicinity can be directly reflected by the hydric and morphological parameters more specifically the specific surface. This parameter, which is inversely proportional to the length, plays an important role in the adsorption problems. As for porosity, sometimes it is necessary to distinguish the accessible surface area and the total surface area including the area of the walls of the pore surfaces. This parameter is strongly dependent on the porosity as shown in Table 3.3.

A material's ability to absorb or release moisture is sometimes called the moisture buffer capacity of the material, and is a function of permeability and the absorptive power of the material. This ability is interesting for example when studying the robustness of a

Table 3.3 Properties of some materials

Materials	Porosity	Specific area (m^{-1})	Permeability (m^2)
Brick	0.12–0.34		4.8×10^{-15} to 2.2×10^{-13}
Granular catalyst	0.45	5.6×10^{7}	
Standard concrete	0.02–0.07		
Fiberglass	0.88–0.93	56×10^{3} to 77×10^{3}	
Sand	0.37–0.50	15×10^{3} to 22×10^{3}	2×10^{-11} to 1.8×10^{-10}
Silica (powder)	0.37–0.49	6.8×10^{5} to 8.9×10^{5}	1.3×10^{-14} to 5.1×10^{-14}

construction against interstitial condensation. Duforestel (1992) proposed an empirical model to calculate the indoor moisture buffer, and classified the hygroscopic materials into two general categories: high absorption and low absorption. The Nordetest protocol proposes to place square samples to the wetting and drying cycles clearly defined (Rode et al., 2007). The moisture-buffering capacity can be determined experimentally by weighing the samples, which are subjected to periodic changes in humidity:

$$\mathrm{MBV}_{8h} = \frac{m_{max} - m_{min}}{A \cdot \left(\mathrm{RH}_{humidification} - \mathrm{RH}_{drying}\right)} \tag{3.13}$$

where m_{max} and m_{min} are the maximum and the minimum water mass accumulated in the sample, respectively, A (m^2) is the exposed specimen surface, $\mathrm{RH}_{humidification}$(%) is the relative humidity applied during the humidification cycle, and RH_{drying}(%) is the applied relative humidity during the drying cycle.

Moisture buffer values (MBVs) using the Eq. (3.13) and the results of successive cycles of wetting and drying (regular weighing was performed for each cycle) are shown in Fig. 3.10 for aerated concrete, oriented strand board (OSB), and wood fibrous insulation (WFI).

According to the MBV classification given by Rode (2005), the buffering effect of building materials can be considered as very important for the durability and for hygrothermal performance of a building. As for thermal diffusivity, the moisture accumulation capacity can be expressed as follows (Hagentoft, 2002):

$$b_m = \sqrt{\frac{\delta_p \cdot \rho_s \cdot \xi}{p_{sat}}} \tag{3.14}$$

b_m (kg/m^2 Pa s$^{0.5}$) is the moisture accumulation capacity, ξ is the slope of the sorption desorption isotherm, ρ_s (kg/m^3) is the dry density of the sample, δ_p (kg/(m s Pa)) is the vapor permeability, and p_{sat} (Pa) is the saturation pressure.

Such a secondary evaluation method is performed by using the moisture accumulation calculated by Eq. (3.14). It is mainly based on the experimental results of sorption desorption isotherms of the studied materials. The results are shown in Fig. 3.11. The

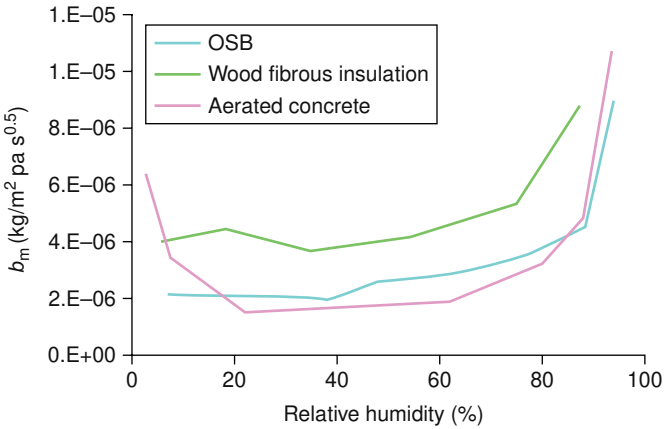

Fig. 3.11 Moisture accumulation capacity b_m as a function of relative humidity (kg/m^2 Pa s$^{0.5}$).

ability of the materials to exchange moisture with the ambient air (ie, buffer capacity) has been explained using two different methods (Eqs. 3.13, 3.14) (Peuhkuri, 2003). The most significant observation is that for both methods, the same classification of the behavior of materials is obtained.

Both buffering capacity assessment methods are adapted to conditions at equilibrium, unlike the dynamic method that has been proposed by Peuhkuri (2003). It was shown that, in general, the moisture-buffering capacity is sometimes underestimated when using equilibrium conditions with respect to the dynamic approach.

7 Durability of bio-based material

In the previous sections, the focus was mainly on the study of the cementitious material's durability as a function of the morphological and the local physical properties. However, nowadays, bio-based materials are becoming increasingly competitive to fully cementitious materials due to their environmental benefits.

Actually, wooden or partially wooden materials present many advantages; in addition to being a 100% renewable resource, wood is a naturally recyclable and biodegradable building material. Compared to other building products like concrete and steel, it has a lower environmental impact (Bribián et al., 2011). Because of their complex morphology and the high heterogeneity of wooden materials, there is still a lack of knowledge concerning their microscopic geometric changes, due to the hygrothermal solicitations. These changes usually lead to a considerable evolution of the resulting thermophysical properties of the material, which constrain its use. Indeed, the latewood/earlywood transition present in the wood structure substantially influences the macroscopic behavior of the material.

In reality, the hygrothermal behavior of wood involves the complex interaction of different heat, air, and moisture transfer mechanisms. At the pore (1–100 μm) scale, the physical transfer as well as the liquid–vapor interface topology and their interactions with the solid matrix make the study of these mechanisms extremely complex. In fact, the macroscopic material's behavior is highly dependent on the mechanisms involved at the microscopic scale. Indeed, the swelling and shrinkage phenomena, observed at the macroscopic scale, is the main evidence reflecting such change caused by the hygric transfer history within the material; unfortunately these dimensionless phenomena are often neglected by the researchers.

Recently, El Hachem et al. (2015) conducted an experimental investigation on spruce wood based on the nondestructive, 3D-imaging technique “X-ray tomography.” This method allows for the locating of any heterogeneity in the material (see Fig. 3.12, obtained at a resolution of $3.35 \times 3.35 \times 3.35\ \mu m^3$ at dried conditions).

The region of interest (ROI) of a dried specimen containing the latewood/earlywood discontinuity is represented in Fig. 3.5 (above section). In both figures, it can be observed that the latewood phase is characterized by the cells containing thicker walls and smaller cavities that become smaller when approaching the latewood/earlywood interface. It can be noticed that the smallest pores belong to the thickest fibers.

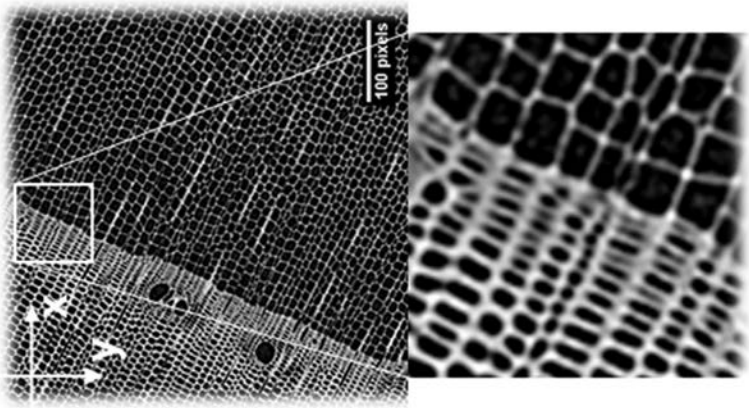

Fig. 3.12 Region of interest of a dried spruce wood specimen in the (*x*,*y*) plane, without the latewood/earlywood interface presence.

El Hachem et al. (2015) confirmed that the presence of the latewood/earlywood discontinuity in the material decreases its porosity from 80% to 50%. In addition to these wooden material's morphological changes and their interaction with mortar on the interface inclusion, these materials are exposed to other risks affecting their durability. Such risks must include several criteria, which make them hazardous; mold growth is one of the most important criteria for the evaluation of the material's degradation since the porous parts of these bio-based materials are continuously exposed to internal and external environmental conditions (see Fig. 3.13).

Currently there are several known adverse health effects due to the exposure to fungi. For example, immunological effects that are associated with allergic reactions, subsequent to the exposure of allergenic proteins; some types of fungi such as, Cladosporium, Alternaria, Penicillium, Aspergillus, are commonly associated with allergies and aggravate rhinitis and asthma (Boudih, 2011). Thus, there is a necessity to examine such fungal phenomenon that may be continuously present in our buildings. Moisture is often the most influential parameter for spore germination and mold growth. Water availability is required for fungi to ensure their physiological and metabolic activities. However, fungal growth depends not only on the ambient relative humidity, but also on the water activity of the substrate.

In this context, the mold-growth behaviors of three wooden material types (massive spruce wood (MSW), WFI, and OSB) are examined. Fig. 3.14 shows an example of mold growth for the MSW, WFI, and OSB samples exposed at a 99.4% of relative humidity in an isothermal desiccator (at 25°C).

After just 1 week of exposure, the contamination surface was visually detected on treated (sterilized) and untreated OSB samples. This is certainly linked to the chemical composition of OSB (its wealth of different types of wood) and its high heterogeneity. It also confirms the results of Lähdesmäki et al. (2011), which assume that fungi prefer to grow on a rougher surface than smooth; the OSB surface is rougher than that

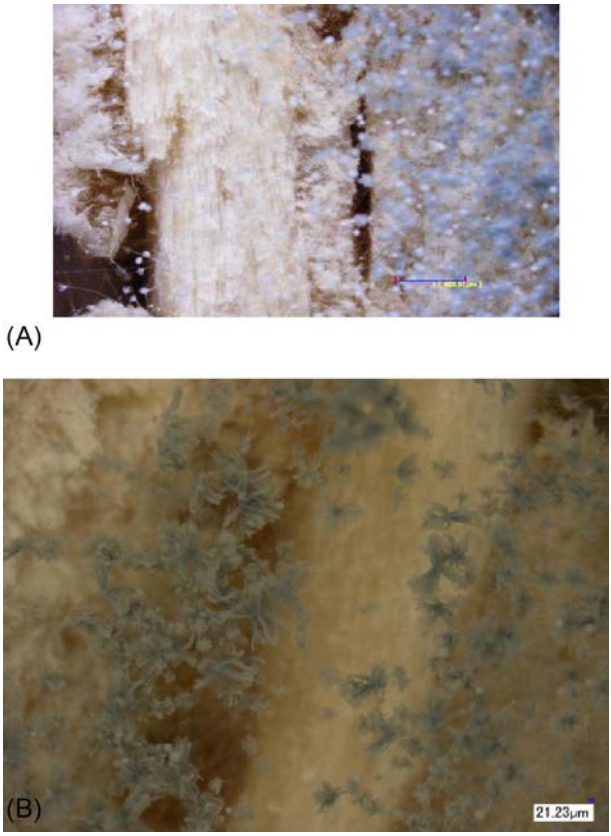

Fig. 3.13 Mold observation for oriented strand board (A) and wood fibrous insulation (B) after 2 weeks of exposure to 80% of relative humidity. Observation under the Keyence microscope.

of WFI and has a rougher surface than that of MSW. The results also confirm that the untreated material is more susceptible to develop fungal compared to those sterilized initially.

High sensitivity to the hydric changes was obtained in particular for OSB, which presents the most heterogeneous composition compared to MSW and WFI; it presents a maximum mold index value (noted *M*) of 6 observed visually at high relative humidity (99%) after only 1 week of exposition, which presents a high risk of early degradation (Fig. 3.14). We indicate here that the index-classification criteria (*M*) have been recently modified to allow its application to the evaluation a large type of materials (Lähdesmäki et al., 2011). For example, mold indexes of 2 signify moderate growth detected with microscopy, and a mold index of 5 signifies a visually detected growth of more than 5%. This parameter can be used as input data for material models (Hukka and Viitanen, 1999) predicting the response of pure-wooden material to arbitrary temperature and humidity conditions.

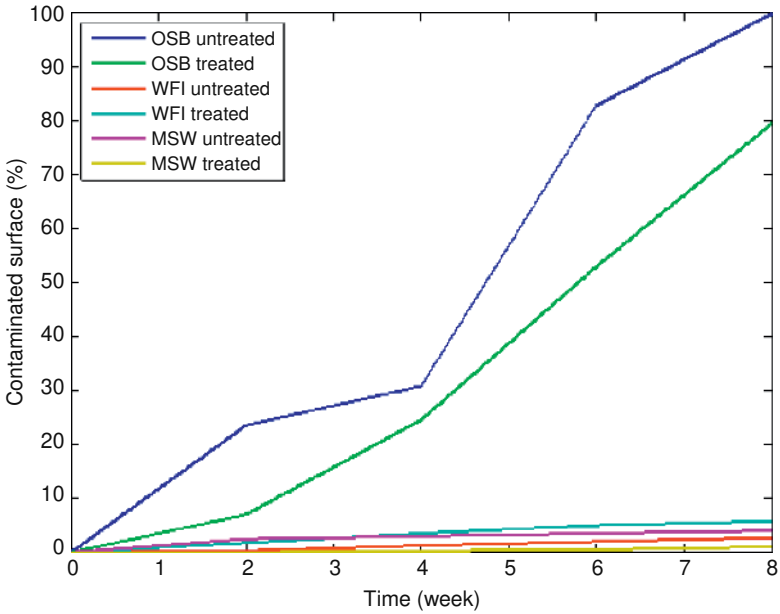

Fig. 3.14 The mold of OSB, WFI, and MSW samples conditioned in transparent desiccator at 99.4%.

3.8 Future trends

This chapter focuses on the effect of physical parameters such as porosity and permeability on the durability and thermal properties of construction materials as well as the effect on the environment and human health.

The amplification of permeability by cracks was also considered. The water-vapor transfer and adsorption phenomena constitute an important characteristic for some materials, and exhibit their great ability in water storage. Such water-storage abilities affect the diffusion phenomena, due to multiphase coupling, and also allow for the interaction of the material with the ambient vicinity. Such interactions provide the environmental-regulation properties (ie, the moisture-buffering capacity) of materials. These parameters characterize the ability of a material to moderate the variations in relative humidity of the surrounding air.

The inclusion of biomaterials increase the complexity of the interaction on a multi-scale and modify the durability task. Such interaction is due to the different time-scale difference and the strong inhomogeneity between the biomaterials and the cement paste. Such inhomogeneity affects the global durability and the water or humidity distribution in such innovative construction materials. Such new problems contribute significantly to fungi development and allow for improved knowledge of fungi's effect on people's health.

References

Adler, R., 2008. Some new random field tools for spatial analysis. Stoch. Env. Res. Risk Assess. 22, 809–822.

Bajja, Z., Dridi, W., Bennacer, R., Darquennes, A., Le Bescop, P., 2015. Link between microstructure and diffusivity in silica fume mortars. In: BMC-11, Pologne–Varsovie, September.

Bejaoui, S., Sercombe, J., Mugler, C., Peycelon, H., 2006. Modelling of radionuclide release from a concrete container. Transp. Porous Media 69 (2007), 89–107.

Benboudjema, F., 2012. Prédiction de la diffusivité effective dans les matériaux à matrice cimentaires: comparaison entre des approches analytiques et numériques. Initial report, Ecole normale supérieure de Cachan, Cachan. Juin.

Bogdan, M., 2015. Modélisation morphologique multi-échelles de matériaux cimentaires—application à la prédiction de propriétés effectives de diffusion (Thèse de doctorat de l'ENS de Cachan).

Bories, S., Mojtabi, A., Prat, M., Ouintard, M., 2008. Transfert de chaleur dans les milieux poreux: changement de phase. Technique de l'ingénieur, BE 8 251.

Boudih, S., 2011. Identification des moisissures et de leurs métabolites secondaires colonisant des supports papiers (Thesis). Paris-Est University, Marne-la-Vallée. HAL Id: tel-00781807.

Bouny, B., 2007. Water vapor sorption experiments on hardened cementitious materials. Part II: essential tool for assessment of transport properties and for durability prediction. Cem. Concr. Res. 37 (3), 438–454.

Bribián, I.-Z., Capilla, A.-V., Usón, A.-A., 2011. Life cycle assessment of building materials: comparative analysis of energy and environmental impacts and evaluation of the eco-efficiency improvement potential. Build. Environ. 46, 1133–1140.

Carcassès, M., Julien, S., Schiettekate, A., 2005. Conclusions on the performance of materials based on CHLORTEST project. In: Resistance of Concrete to Chloride Ingress, From Laboratory to In-field Performance, Alicante, 1–2 December.

De Larrard, T., 2010. Variabilité des propriétés du béton: caractérisation expérimentale et modélisation probabiliste de la lixiviation (Thèse de doctorat de l'ENS de Cachan).

Djerbia, A., Bonneta, S., Khelidj, A., Baroghel-bouny, V., 2008. Influence of traversing crack on chloride diffusion into concrete. Cem. Concr. Res. 38 (6), 877–883.

Duforestel, T., 1992. Bases métrologiques et modèles pour la simulation du comportement Hygrothermique des composants et ouvrages du bâtiment (Thèse de Doctorat). Ecole Nationale des Ponts et Chaussées, Champs-sur-Marne.

El Hachem, C., Abahri, K., Bennacer, R., 2015. 3D X-ray tomography for the hygrothermal characterization of spruce wood. In: First International Conference on Bio-based Building Materials, ICBBM, June 22nd–24th, 2015, Clermont-Ferrand, France.

Garboczi, E.J., Bentz, D.P., 1992. Computer simulation of the diffusivity of cement-based materials. J. Mater. Sci. 27, 2083–2092.

Hagentoft, C., 2002. HAMSTAD Final Report: Methodology of HAM-Modeling. Report R-02:8, Department of Building Physics, Chalmers University of Technology, Gothenburg.

Hukka, A., Viitanen, H.A., 1999. A mathematical model of mould growth on wooden material. Wood Sci. Technol. 33, 475–485.

International Energy Agency (IEA), 2007. Experimental analysis of moisture buffering. Annex 41, Subtask 2. http://www.ecbcs.org/annexes/annex41.htm.

Jennings, H.M., 2008. Refinements to colloid model of C-S-H in cement. Cem. Concr. Res. 38 (3), 275–289.

Kaviani, M., 1991. Principles of Heat Transfer in Porous Media. Springer Verlag, New York, NY.

Lähdesmäki, K. et al., 2011. Mould growth on building materials in laboratory and field experiments. In: 9th Nordic Symposium on Building Physics—NSB. Finland, June.

Mejlhede Jensen, O., Freiesleben Hansen, P., Coats, A.M., Glasser, F.P., 1999. Chloride ingress in cement paste and mortar. Cem. Concr. Res. 29, 1497–1504.

NF X 50-501, 1982. Durée de vie et durabilité des biens—Vocabulaire des activités de rénovation et de reconstruction—États de référence des biens de réemploi—Norme expérimentale, février.

Ngala, V.T., Page, C.L., Parrott, L.J., Yu, S.W., 1995. Diffusion in cementitious materials. II. Further investigations of chlorides and oxygen diffusion in well cured OPC and OPC/30%PFA pastes. Cem. Concr. Res. 25, 819–826.

Nonat, A., 2004. The structure and stoichiometry of C-S-H. Cem. Concr. Res. 34 (9), 1521–1528.

Ollivier, J.-P., Torrenti, J.-M., 2008. La structure poreuse des bétons et les propriétés de transfert, dans la durabilité des bétons, sous la direction de J.-P. Ollivier et A. Vichot. Presse de l'ENPC, Paris.

Peuhkuri, R., 2003. Moisture Dynamics in Building Envelopes (Ph.D. thesis). Department of Civil Engineering, Technical University of Denmark, Kongens Lyngby.

Rastiello, G., Bennacer, R., Nahas, G., Bogdan, M., 2015. Effective permeability and transfer properties in fractured porous media. Defect Diffus. Forum 362, 172–189.

Richet, C., 1992. Etude de la migration des radioéléments dans les liants hydrauliques—Influence du vieillissement des liants sur les mécanismes et la cinétique des transferts (Ph.D. thesis). Paris XI Orsay, Orsay.

Richet, C., Pin, M., Maury, J., Lalle, J.P., Fockedey, C., Adenot, F., Aspart, A., 1997. Amélioration de la fiabilité du modele diffusion. Note Technique, N.T. SESD/97.37.

Rode, C., 2005. Moisture Buffering of Building Materials. 1601-2917 Nordisk Innovations center, Kongens Lyngby, ISBN: 87-7877-195-1 BYG R-126.

Rode, C., Peuhkuri, R., Time, B., Svennberg, K., Ojanen, T., 2007. Moisture buffer value of building materials. J. ASTM Int. 4 (5), 1–12.

Roubinet, D., Liu, H.-H., de Dreuzy, J.-R., 2010. A new particle-tracking approach to simulating transport in heterogeneous fractured porous media. Water Resour. Res. 46, W11507.

Tang, L., 2003. Chloride Ingress in Concrete Exposed to Marine Environment-Field Data Up To 10 Years Exposure. SP report 2003:16, Building Technology, Swedish National Testing and Research Institute, Boras.

Tits, J., Jakob, A., Wieland, E., Spieler, P., 2003. Diffusion of tritiated water and $22Na^+$ through non-degraded hardened cement pastes. J. Contam. Hydrol. 61 (1–4), 45–62.

Tognazzi, C., 1998. Couplage fissuration-dégradation chimique dans des matériaux cimentaires: caractérisation et modélisation (Thèse de doctorat). INSA Toulouse, Toulouse.